agronomy

MDPI

Article

Experimental Investigation of Water Infiltration Law in Loess with Black Locust (*Robinia pseudoacacia*) Roots

Qi Gu [1,2], Tianfeng Gu [1,2,*], Dengfei Zhang [1,2], Jiading Wang [1,2] and Tao Xiao [1,2]

[1] State Key Laboratory of Continental Dynamics, Northwest University, Xi'an 710069, China; 202010343@stumail.nwu.edu.cn (Q.G.); dfzhang87@nwu.edu.cn (D.Z.); wangjd@nwu.edu.cn (J.W.); axiao@chd.edu.cn (T.X.)
[2] Department of Geology, Northwest University, Xi'an 710069, China
* Correspondence: gutf@nwu.edu.cn (T.G.)

Abstract: Physical model experiments are increasingly applied in the study of the water infiltration law in loess with roots. In the past, due to differences in study objects and the limitations of measuring techniques, the infiltration law in loess with roots is rarely evaluated by using appropriate indoor physical model experimental data. In order to investigate the law of water infiltration in loess with roots, we designed a new soil column experimental device that can automatically collect data and images. By comparing the soil column experiment data of loess, we analyzed variables in root contents (the ratio of root mass to dry soil mass) and root types. Roots with diameters of 0–2 mm, 2–5 mm, and 5–10 mm are defined as type I, type II, and type III, respectively. It was found that the water infiltration rate, water-holding capacity, and saturated permeability coefficient increase with the increase in root content. In loess containing different root types, the root types were found to improve the rate of water infiltration, water-holding capacity, and saturated permeability coefficient in the soil. The root types were ranked in descending order in terms of their impact: root type II had the highest improvement, followed by root type III, and then root type I. The phenomenon of circumferential flow existed when water infiltrated loess with roots. Root content and root type would affect the radius of circumferential flow, infiltration path, and cross-section. When calculating the saturated permeability coefficient of loess with roots, ignoring the effect of circumferential flow would lead to a higher result.

Keywords: loess; *Robinia pseudoacacia*; root; water infiltration; saturated permeability coefficient

check for updates

Citation: Gu, Q.; Gu, T.; Zhang, D.; Wang, J.; Xiao, T. Experimental Investigation of Water Infiltration Law in Loess with Black Locust (*Robinia pseudoacacia*) Roots. *Agronomy* **2024**, *14*, 276. https://doi.org/10.3390/agronomy14020276

Academic Editor: Ivan Francisco Garcia Tejero

Received: 19 December 2023
Revised: 18 January 2024
Accepted: 24 January 2024
Published: 26 January 2024

Copyright: © 2024 by the authors. Licensee MDPI, Basel, Switzerland. This article is an open access article distributed under the terms and conditions of the Creative Commons Attribution (CC BY) license (https://creativecommons.org/licenses/by/4.0/).

1. Introduction

The plateau serves as a critical zone for soil formation and nutrient cycling, which supports diverse agricultural practices. Its vegetation cover plays an essential role in reducing soil erosion, one of the most pressing environmental issues on the plateau. Rainfall infiltration is the main source of soil water replenishment in the Loess Plateau, which affects vegetation growth, crop yield and groundwater replenishment [1–4]. Infiltration is the process by which surface water enters the soil after precipitation or artificial water application. Infiltration channel changes are mainly due to changes in the spatial distribution and configuration of plant roots [5]. Due to such changes, it is quite difficult to accurately describe the infiltration path, infiltration rate, and distribution of water in soil [6–8]. Notably, such changes also bring certain difficulties in water management and efficient utilization of water resources during crop growth [9]. Therefore, it is necessary to purposefully explore the law of water infiltration in vegetation root loess.

The law of water infiltration in loess with roots is often studied by field experiments and laboratory tests [10–13]. Many soil infiltration measurement methods have been developed and used, such as the double-rings method, cutting-ring method, disc permeometer, and rain simulator [14–18]. The disadvantages of the double-rings method are as follows:

firstly, it is impossible to obtain higher initial permeability under insufficient water supply; secondly, the double rings inserted into the soil surface can easily disturb the topsoil and crust on the soil surface; thirdly, this method can only test the penetration into surface soil, not into deep soil [19]. The disadvantages of the cutting-ring method mostly lie in the small size of loess samples and the lack of typicality [20]. The initial infiltration of soil is related to rainfall intensity. However, the rain simulator cannot reflect the actual rainfall, so the measured value does not represent soil permeability [21]. When using a disc permeometer for an infiltration test, possible water leakage may negatively affect the accuracy of the measured results [22].

Since 1950, numerous articles have been published in the fields of hydrogeology, agriculture. and soil science, which largely rely on the results obtained from soil column experiments [23–25]. In this way, water forms a certain moist zone along the soil surface, which progressively extends to the final moist zone over time. When the investigators determined the hydraulic characteristics using the point source method, they found that the infiltration process in loess with a single-point water supply could be divided into four stages: fast infiltration, steady infiltration, slow infiltration, and optimal infiltration [26,27]. Their measurements were made after equilibrium conditions occurred, so only the final radius and equilibrium permeability were observed. Vegetation will affect the infiltration of loess with roots [28], and the degree of its effect is closely related to the type of vegetation and the number of roots [29]. However, previous studies mostly focused on the effects of soil characteristics and root biomass on the whole infiltration process [30–33], while the effects of root diameter and root content on law of water infiltration in loess remain to be studied.

In this study, a laboratory soil column experiment was conducted on loess with roots, and water infiltration into loess with roots was quantitatively studied. *Robinia pseudoacacia* is extensively cultivated worldwide due to its adaptability and rapid growth, particularly in the environmentally vulnerable Loess Plateau region [34,35]. It plays a crucial role in soil improvement and the restoration of degraded land. The availability of root samples from *Robinia pseudoacacia* in this region facilitates the study of soil hydraulic properties. While research on *Robinia pseudoacacia* has primarily focused on its ecological benefits and impact on biodiversity, there remains a gap in our understanding of its effects on soil hydrological processes [36–39]. In summary, this study aims to (1) develop a seepage device that can dynamically measure and record the shape and position of the wetting front, water content, and saturated permeability coefficient in loess in real time; (2) determine the effect of root diameter and root content on soil permeability; and (3) determine the effect of "circumferential flow" on the saturated permeability coefficient of loess when water infiltrates into the root. This study can provide an opportunity to clarify the effect of root diameter and root content on the infiltration law in loess, and also offer new insights into the effect of "circumferential flow" on the saturated permeability coefficient of soil. Based on these findings, it is easier to understand the law of water infiltration in loess with roots, which is still to be revealed.

2. Materials and Methodology

2.1. Site Description and Soil Properties

The *Robinia pseudoacacia* roots and loess samples used in this experiment were all from Qiulin Town, Yichuan County, Yan'an City, Shaanxi Province, China (36°7′54″~36°7′56″, 110°15′14″~110°15′16″), as shown in Figure 1A. This area belongs to a continental monsoon climate, with an average temperature of about 22~27 °C in summer and about −4~4 °C in winter, and an annual total precipitation of 130~998 mm.

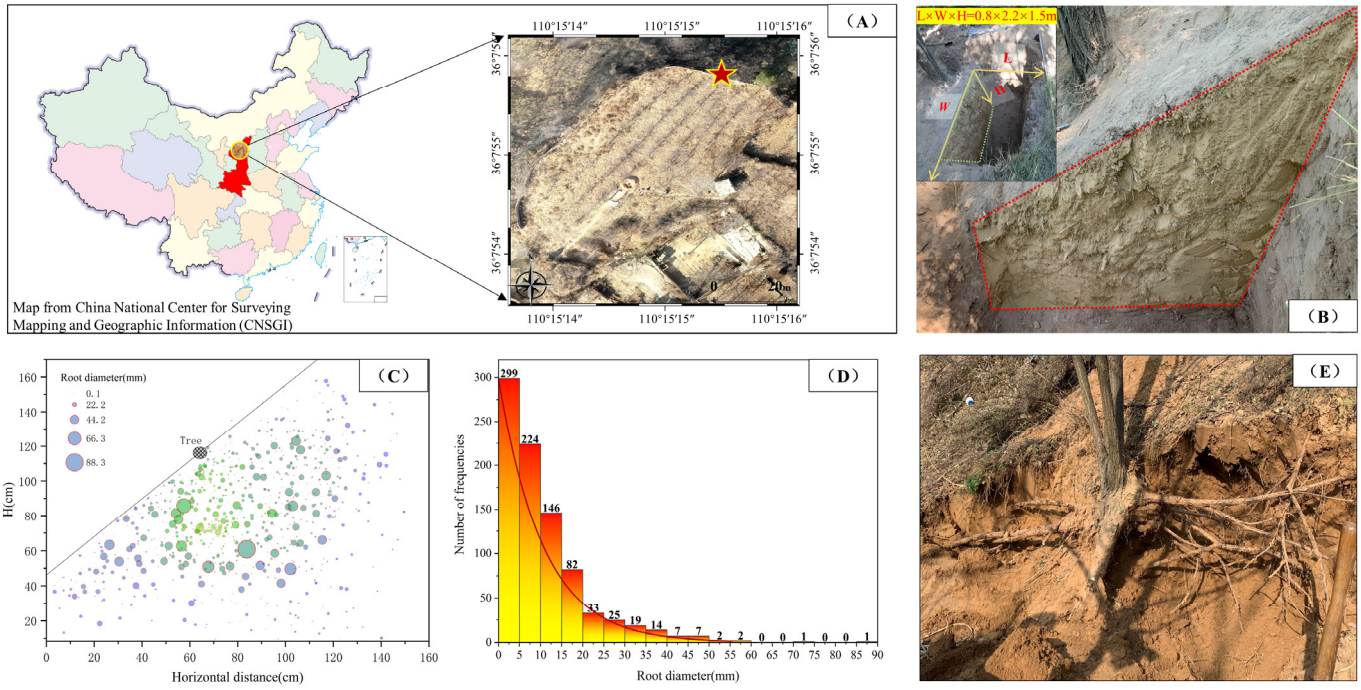


Figure 1. The location of the study area and distribution characteristics of roots in the loess profile: (**A**) the location of the study area; (**B**) the excavation of trenches and the acquisition of root-containing soil profiles; (**C**) the distribution characteristics of roots in the loess profile; (**D**) the variation of the number of thick and fine roots in all root samples; and (**E**) site sampling by whole-plant excavation.

Loess samples were collected near the rhizosphere of *Robinia pseudoacacia* with a depth of 10–50 cm. According to recommended methods, the basic physical and mechanical indicators of loess samples were measured (Table 1). Soils were characterized for indicators and engineering properties according to the Unified Soil Classification System (USCS). Atterberg limits of the soil were obtained as the liquid limit (28.14%) and plastic limit (16.82%). The soil belongs is categorized as sandy silt [40].

Table 1. The main physical properties of the studied loess soil.

Sample	w (%)	G_s	ρ (g/cm^3)	ρ_d (g/cm^3)	e	w_L (%)	w_p (%)	I_p (%)	ρ_r (g/cm^3)	Classification
Malan Loess	12.50	2.70	1.69	1.30	0.82	28.14	16.82	12.32	1.2	Sandy silt

w: water content, G_s: specific gravity of soil grain, ρ: natural density, ρ_d: natural dry density, e: void ratio, w_L: liquid limit, w_p: plastic limit, I_p: plasticity index, ρ_r: plant root density.

In order to simulate the site experiment environment as much as possible, the loess samples retrieved from the field were processed by the following steps. Firstly, the retrieved disturbed soil samples were air-dried, crushed, screened (using a sieve 2 mm in diameter), and dried (at 105 °C). Secondly, the dried soil was mixed with water to achieve the target water content. In order to distribute water evenly in the soil, the wet soil samples were placed in a fresh-keeping device for 72 h. Finally, soil samples with target water content were filled into containers with a thickness of 5 cm per layer.

2.2. Distribution Characteristics of Roots and Collection of Samples

The roots of *Robinia pseudoacacia* were investigated in situ by the trenching method, as shown in Figure 1B. The results show that the roots were mainly distributed horizontally in the soil, and the number of roots increased first and then decreased with the increase in depth. Among all the roots counted, fine roots had the highest proportion, while thick

roots had the lowest, with diameters ranging from 0.1–10 mm, as shown in Figure 1C,D. In order to describe the root density quantitatively, the concept of root content (the ratio of root mass to dry soil mass per cubic decimeter) was introduced. The root content of soil in the trench section ranged from 0.23% to 2.11%, with an average of 1.17%; the dry density of loess with roots was 1.3 g/cm^3.

Root samples were collected by the whole-plant excavation method, as shown in Figure 1E. Complete and undamaged root samples were carefully selected. In order to facilitate sampling and transportation, all roots were uniformly cut to 50 cm in length. In order to prevent the loss of water and the destruction of root tissue during transportation, the root samples were packed by layering with plastic wrap and bubble film.

2.3. Design of Experiment Scheme

According to the field investigation and previous classification of root diameter, the roots with diameter in the range of 0–10 mm were divided into three categories: 0–2 mm, 2–5 mm and 5–10 mm, denoted type I, type II and type III, respectively [41]. The root content (k_r) in the range of 0.23–2.11% was refined to 0.23%, 1.17%, and 2.11%. Experiments were designed by the orthogonal method, and a group of loess was added as blank control group, with 10 groups in total. The experimental instrumentation was a seepage model device. The initial water content of the soil was 12.5%, while the dry density was 1.3 g/cm^3. The roots were laid horizontally in the soil.

2.4. Experimental Instrumentation and Main Operation Steps

The seepage experimental instrumentation consisted of a cuboid transparent container (made of acrylic material), data acquisition device, image acquisition device, and water supply device (Figure 2). The thickness of the plates at the bottom and around the transparent container was 2.0 cm and 1.0 cm, respectively, and the size was 44 × 10 × 70 cm (L × W × H). Each plate surface was connected by acrylic glue. A steel ruler (0.1 mm in accuracy) was fixed on the right side of the container. One MT10 water sensor (accuracy ±3%) was installed every 10 cm on the right and back sides of the container, with a total of six sensors. The distance between the sensors on the right and back sides was 5 cm from a one-dimensional viewing angle. A water outlet with a diameter of 2 cm was arranged at the lower right of the container, and the outflow water was collected in a glass bottle with a diameter of 15 × 20 cm (D × H). The glass bottle was located on the loading plate (the loading plate was made of a 304 stainless steel grid, with a 20 × 20 cm frame and 2 cm mesh), which was connected to a YBY-50N tension sensor (80 μv/N in sensitivity) through a steel wire rope with a diameter of 0.5 mm. A Campbell CR3000 Data Acquisition System and DH3818Y Static Stress–Strain Measurement and Analysis System were used to collect the data on a water sensor and tension sensor. A Hikvision camera and video recorder were used to photograph and record the water seepage process. In order to keep the head height constant throughout the experiment, an overflow port with a diameter of 3 cm was arranged at the upper left of the transparent container. The main steps of the loess with roots seepage experiment are as follows:

(1) The root and loess were layered into a transparent container, and a gravel layer with a thickness of 2 cm was laid on the top to prevent water flow from scouring the soil surface;
(2) All sensors were connected to their corresponding acquisition systems, and the sampling frequency was set to 1/s;
(3) In order to ensure the uniformity of water content in loess with roots at different depths and the uniqueness of soil initial water content, a real-time monitoring method was adopted to ensure that the volume water content of soil at different depths was kept at 9.6% before water infiltration into loess with roots. This operation aimed to (1) verify whether the target water content of soil is consistent with the monitoring results; (2) facilitate the observation of the time when water sensors at different

positions first sense water; (3) conduct a quantitative analysis of the change in soil water content;

(4) Open the external water source-regulating valve and adjust the water flow, and open the drainage hole at the upper left, so that the water head height reaches the target value;

(5) Open the data and image acquisition system, and record the data changes on the sensor, as well as the position and shape of the wetting front, in real time.

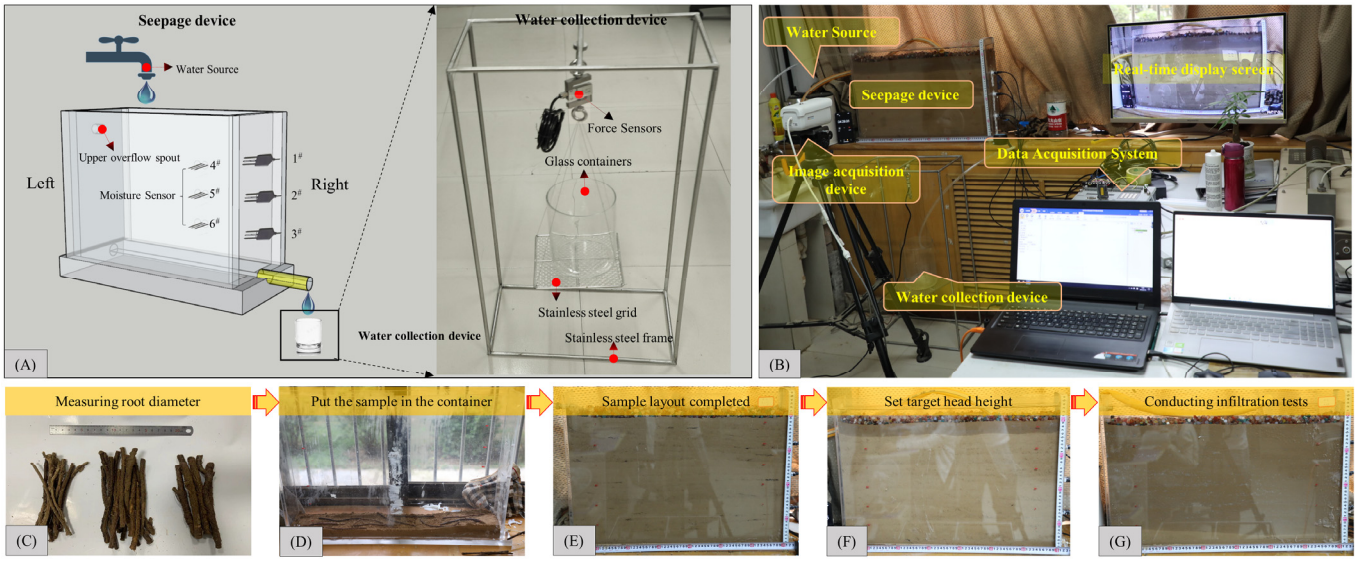


Figure 2. Seepage device and its main operational steps: (**A**) seepage device and water collection device; (**B**) experiment scenes when different devices are connected together; (**C**) measuring root Diameter; (**D**) put the sample loess in containers; (**E**) sample layout completed; (**F**) setting target head height; (**G**) conducting infiltration tests.

2.5. Determination of Infiltration Rate and Saturated Permeability Coefficient

The average rate of water infiltration was measured by visual observation and water sensor monitoring. In visual observation, the migration distance of the wetting front was measured with a steel ruler, and the time was recorded by video equipment. The ratio of the migration distance of the wetting front to the time consumed is the average rate of water infiltration. The shape and position of the wetting front at different times were captured by PotPlayer software (Version: 220420). Assuming that the height of the root-containing soil in the transparent container is H_0 (cm), and the wetting front migrates to H_i after t (min), where i represents the change in the position of the wetting front, the average infiltration rate is expressed as

$$v_i = \frac{H_0 - H_i}{t_i} \quad (1)$$

The position of the water sensor is constant in the transparent container. If the time taken for water to travel from one sensor to another is obtained, the average rate of water infiltration can be calculated. Assuming that the time taken for water to travel from j (1, 2, 3, 4, 5, 6) to m (1, 2, 3, 4, 5, 6) ($m > j$) is t (min), the average flow rate of water between any two sensors is expressed as

$$v_{jm} = \frac{L_j - L_m}{t_j m} \quad (2)$$

The phenomenon of "circumferential flow" occurs when water infiltrates into loess with roots. When evaluating the impact of this phenomenon on the saturated permeability coefficient of the soil, two different calculation methods should be considered:

(1) One in which the effect of "circumferential flow" on the saturated permeability coefficient of the specimen is not considered:

In loess with roots, the seepage length L = 40.0 cm, the total head loss h = 5.0 cm, and the cross-sectional area perpendicular to the flow direction A = 68 cm × 8.5 cm = 578.0 cm^2. When the loess with roots is saturated, the force F (N) displayed on the tension sensor represents the gravity of water. Assuming that in t seconds, the flow rate of water = Q (cm^3/s), the density $\rho = 1.0 \times 10^3$ kg/m^3, the mass = M (kg), the volume = V (cm^3), and the acceleration of gravity g = 9.81 N/kg, according to the force–balance principle and Darcy's law, Equations (3) and (4) can be obtained:

$$Q = \frac{V}{t} = \frac{KAh}{L} \tag{3}$$

$$F = Mg = \rho Vg \tag{4}$$

From Equations (3) and (4), the calculation Equation (5) of the saturated permeability coefficient K can be obtained. In addition, the units for factor 1.41 are cm/N.

$$K = \frac{FL}{Ah\rho gt} = 1.41\frac{F}{t} \tag{5}$$

When the soil in the transparent container is unsaturated, no water enters the collection bottle, and the force on the tension sensor is 0, as shown in Figure 3A. When the soil is saturated, water will enter the collection bottle at the bottom, and the force on the tension sensor will increase over time, as shown in Figure 3B. Notably, the force F is directly proportional to time in this process. Assuming a coefficient k, Equation (5) is simplified as

$$K = 1.41k \tag{6}$$

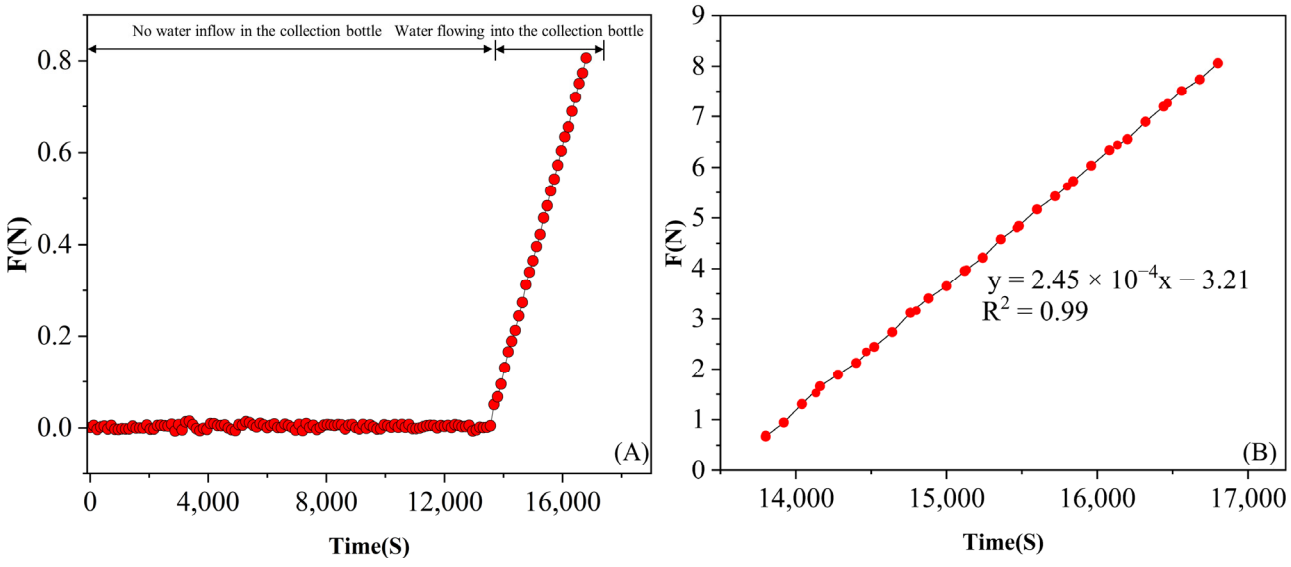


Figure 3. Variation in tension force over time during water infiltration in the specimen with type II roots and a root content of 1.17%: (**A**) changes in tension force over time; and (**B**) variations in tension force overtime after the specimen is saturated.

(2) One in which the effect of "circumferential flow" on the saturated permeability coefficient of the specimen is taken into account:

Since "circumferential flow" may lead to changes in the seepage path and cross-section, only the seepage path of water in loess and the cross-sectional area perpendicular to the flow direction are changed in the analysis, while other parameters remain the same as in

Method 1. For the convenience of analysis, the curvature of the root is ignored during "circumferential flow" around the root. It was assumed that the radius of "circumferential flow" = D (root diameter), the length = 15 cm, root mass = M_r, and root density = ρ_r (constant) in all root types. During each test, the roots were evenly divided into four layers in the soil. According to the conversion relationship between dry soil (M_s) and root content, the mass M_4 of each layer of roots is expressed as

$$M_4 = \frac{M_S \times k_r}{4} \tag{7}$$

Assuming that diameter of each root is D, the mass of the root is expressed as

$$M_{\mathrm{r}} = \frac{15 \times \pi \times D^2 \times \rho_r}{4} \tag{8}$$

The number of roots N in each layer is expressed as

$$N = \frac{M_4}{M_r} = \frac{M_S \times k_r}{15 \times \pi \times D^2 \times \rho_r} \tag{9}$$

The area of roots S_r in each layer is expressed as

$$S_r = 15 \times D \times \frac{M_S \times k_r}{15 \times \pi \times D^2 \times \rho_r} = \frac{M_S \times k_r}{\pi \times D \times \rho_r} \tag{10}$$

When the saturated permeability coefficient is calculated by using Equations (5) and (6), the saturated permeability coefficient of loess with roots is calculated as follows:

$$K' = K + K_r = \frac{F(L - 4D)}{Ah\rho gt} + \frac{2\pi FD}{(A - S_r)h\rho gt} = \left(\frac{L - 4D}{A} + \frac{2\pi D}{(A - S_r)}\right)\frac{F}{h\rho gt} \tag{11}$$

3. Results

3.1. Migration Characteristics of Wetting Fronts during Water Infiltration

Figure 4A,B show the shape and position of wetting front in loess and loess with roots every 10 min. It can be found that the wetting front migrates downward in a straight line at any time when water infiltrates into loess. When water infiltrates into loess with roots, the wetting front migrates downward in an approximately straight line, but the wetting front migrates in a curved shape around the root. In order to clearly observe the shape of wetting front at local zero flux, we selected the typical shape of the wetting front at local position and enlarged it. As illustrated in Figure 4C, our observations indicate a consistent linear migration of the wetting front during water infiltration into loess, which occurs even over limited spatial extents. In Figure 4D, there is a phenomenon of "circumferential flow" during the migration of the wetting front in loess with roots. By comparing the water infiltration phenomena in loess and loess with roots, we observe that in loess with roots, water exhibits a "circumferential flow" phenomenon.

Figure 5 shows the variation characteristics of migration velocity in the wetting front over time under different working conditions. Obviously, the wetting front migration rate varied in the range of 0–1.5 cm/min. Under a single working condition, the migration rate of the wetting front changes with nonlinear characteristics. In order to describe such change quantitatively, we used a logarithmic function to transform the migration rate of the wetting front into a linear state, and divided the migration rate of the wetting front into four stages with increments of 0.2 cm/min in the whole seepage process. (1) In the rapid growth stage, the wetting front migration rate increased sharply and reached its maximum value (1–1.5 cm/min) within 5 min. (2) In the rapid decrease stage, the wetting front migration rate decreased from the previous maximum value to 0.8 cm/min, and this phase lasted for approximately 15 min. Additionally, compared to loess, the wetting front migration rate in loess containing type I roots, type II roots, and type III roots was reduced

by approximately 10 min, 5 min, and 5 min. (3) In the slow decrease stage, the wetting front migration rate gradually decreased from 0.8 cm/min to 0.45 cm/min. Similarly, the wetting front migration rate in loess containing type I roots, type II roots, and type III roots was reduced by approximately 10 min compared to loess. In the steady stage, the wetting front migration rate gradually decreased from 0.45 cm/min to 0.2 cm/min. (4) In the smooth stage, the wetting front migration rate decreased to 0.2 cm/min and remained unchanged until the end of the experiment.

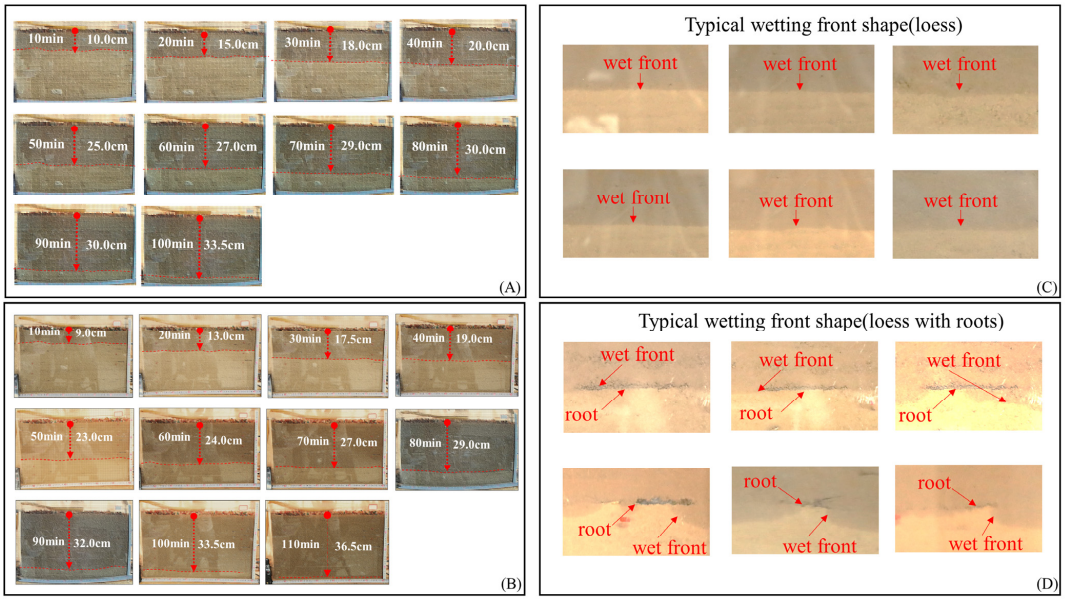


Figure 4. Morphology of the wetting front during water infiltration: (**A**) migration process of the wetting front in loess and (**B**) loess with roots (type I, with a root content of 2.11%); (**C**) local enlarged diagram of the wetting front in loess; and (**D**) local enlarged diagram of the wetting front in loess with roots.

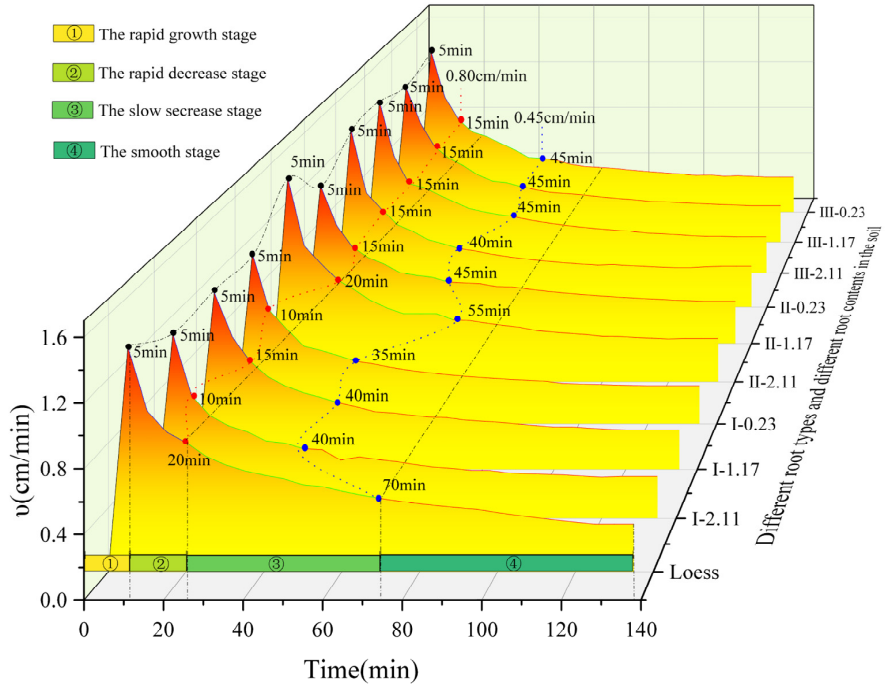


Figure 5. Variation in the migration velocity of the wetting front over time with different root contents and root types.

The average water infiltration rate used as a quantitative measure to the water permeation process and categorize it into four stages. When the root content of loess is constant and the root types change, the average migration rate of the wetting front is the highest in type II root soil with a root content of 2.11%, where the rate is 0.50 cm/min; meanwhile, the average migration rate of the wetting front is the lowest in type I root soil with a root content of 0.23%, in which the rate is 0.27 cm/min. Although the average migration rate of the wetting front in loess has maximum and minimum values, their values are very close, and the difference ranges between 0.02–0.05 cm/min, as shown in Figure 6A–C. It can be seen that root type has little effect on the migration rate of the wetting front. When the root type in soil is constant and the root content changes, the average migration rate of the wetting front will increase with the increase in root content, as shown in Figure 6D–F. Among all the working conditions, the average migration rate of wetting front in the loess with a root content of 0.23% is the smallest, and the value ranges from 0.27 cm/min to 0.30 cm/min. The average migration rate of the wetting front is the largest in the loess with a root content of 2.11%, and the value ranges from 0.32 cm/min to 0.50 cm/min.

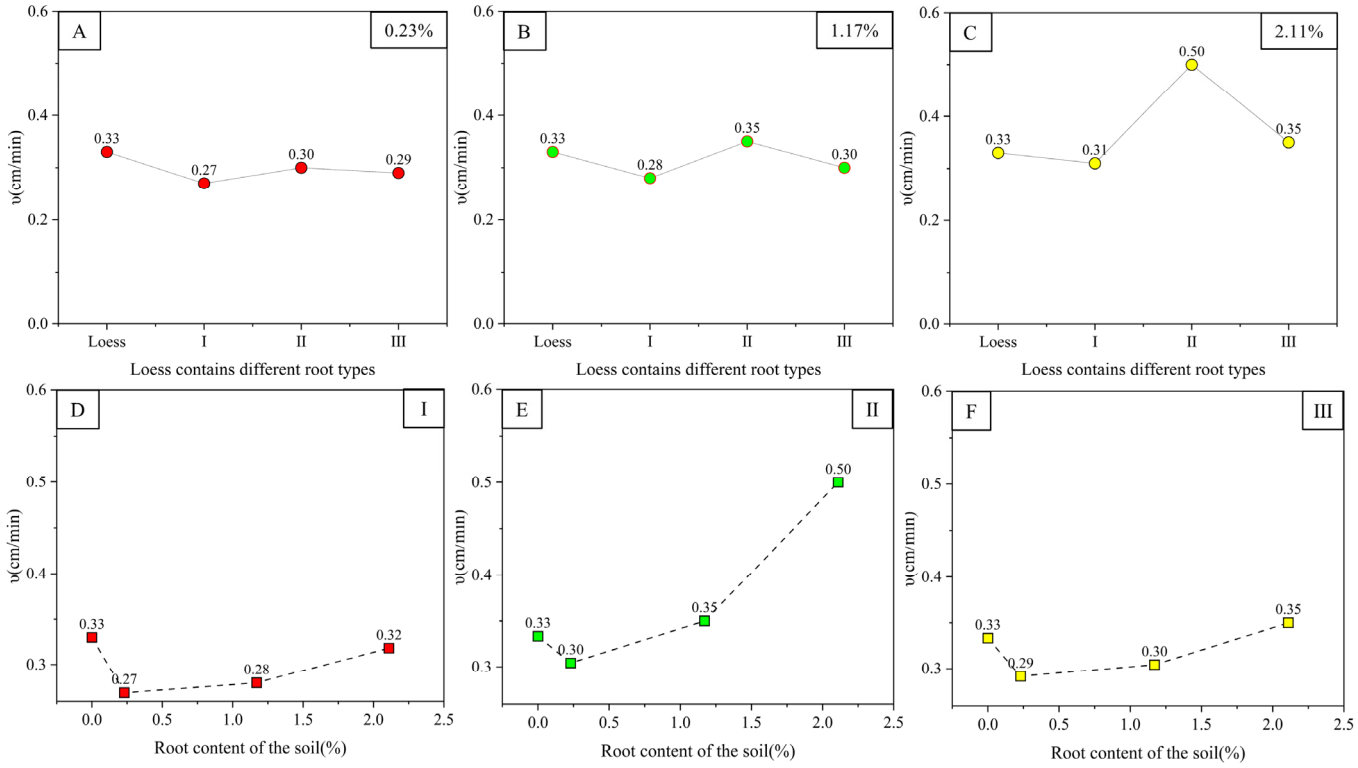


Figure 6. Variation characteristics of the average migration rate of the wetting front under different conditions. The changing characteristics of the migration rate of the wetting front in soil with different root contents (**A**–**C**) and root types (**D**–**F**).

3.2. Characteristics of Water Variation within Root–Soil Combinations

Figure 7 shows the variation characteristics of the internal moisture of loess with type I roots at different depths with different root contents. It can be seen from Figure 7 that the time taken by the sensor to sense the moisture for the first time (as well as changes in moisture) will vary with the depth. At the same depth, the soil moisture changes show trends of increasing first and then stabilizing. Although the distance between sensors is constant, the time taken by water sensors at different depths to sense water changes is different. The starting points of water sensors at different depths can be connected to judge the infiltration characteristics of water in soil according to the connecting characteristics. Curve numbers ①, ②, ③ and ④ in the figure are the working conditions of loess and root-containing soil with root contents of 0.23%, 1.17% and 2.11%, respectively, and the

shape of the line segments in ① is curved, which shows that water in soil infiltrates at a non-uniform velocity. The line shape in ②, ③, and ④ is an oblique and approximately straight line, which shows that the infiltration of water in soil is relatively uniform.

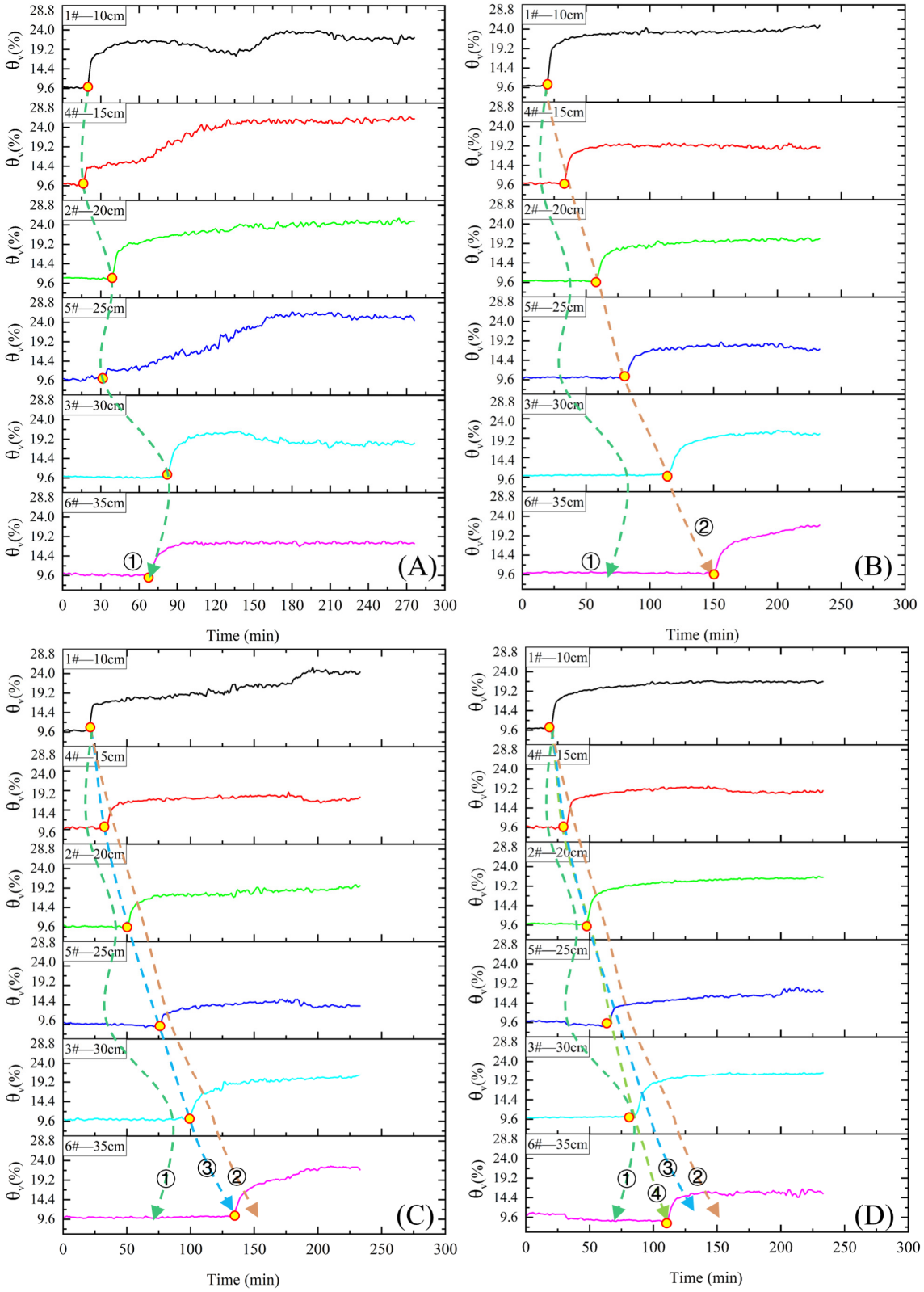


Figure 7. Variation characteristics of volumetric water content in soil with type I roots at different times (loess with root content of (**A**) 0%, (**B**) 0.23%, (**C**) 1.17% and (**D**) 2.11%).

By applying the method of calculating the slope of a straight line, the tangent value of the sharp angle between the extension line of each connecting line and the time axis is the average infiltration rate of water, and its relationship is described as ① > ④ > ③ > ②, which shows that the infiltration rate of loess is the largest, followed by loess with root content of 2.11%, 1.17%, and 0.23%. Certainly, as the root content increases in loess containing type I roots, the average rate of infiltration in such soils also increases. This result is consistent with the results described in Section 3.1. The infiltration characteristics of loess with type II and type III roots with different root contents were studied with the same method, and similar results were obtained, as shown in Figures 8 and 9.

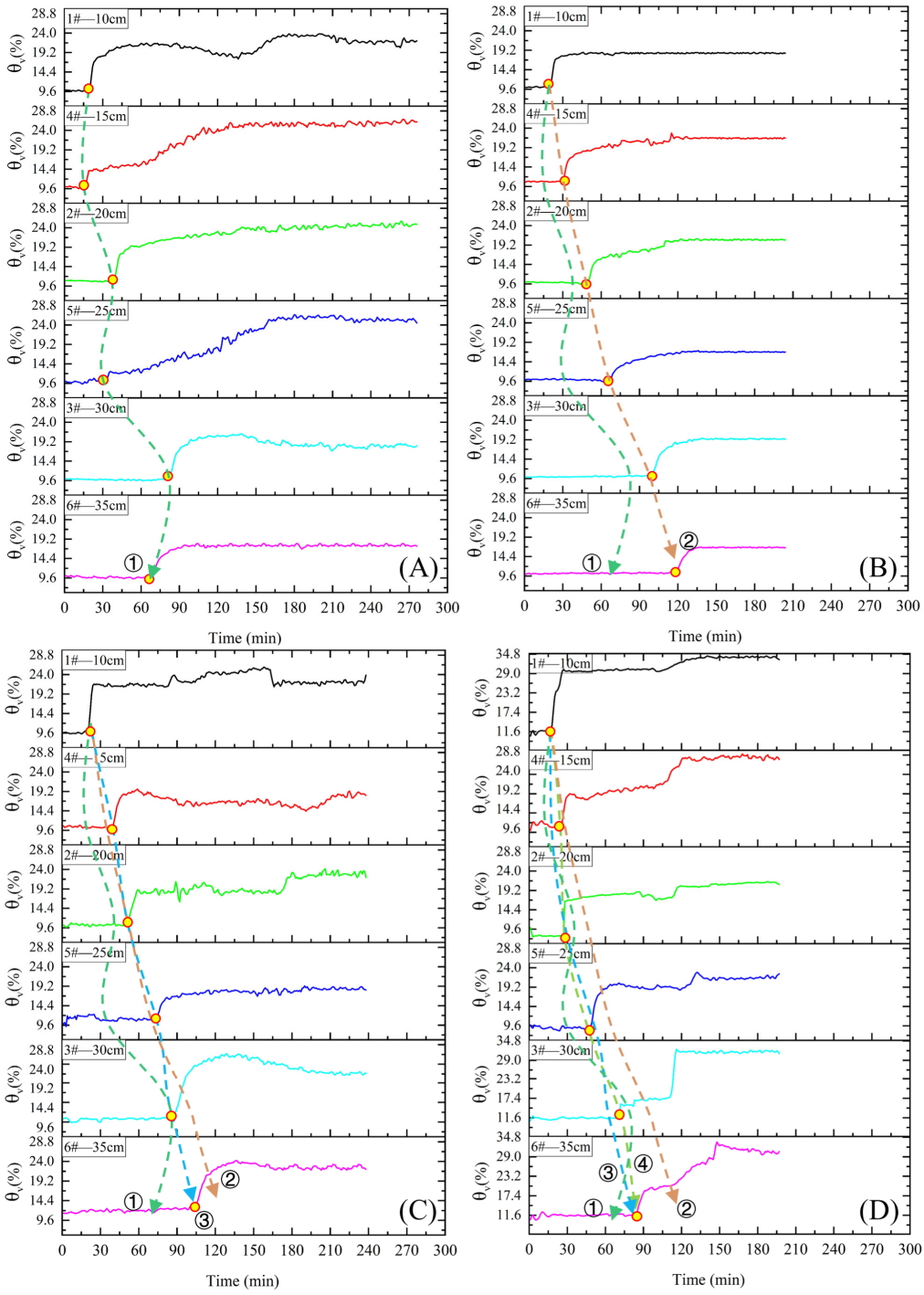


Figure 8. Variation characteristics of volumetric water content in soil with type II roots at different times (loess with root content of (**A**) 0%, (**B**) 0.23%, (**C**) 1.17% and (**D**) 2.11%).

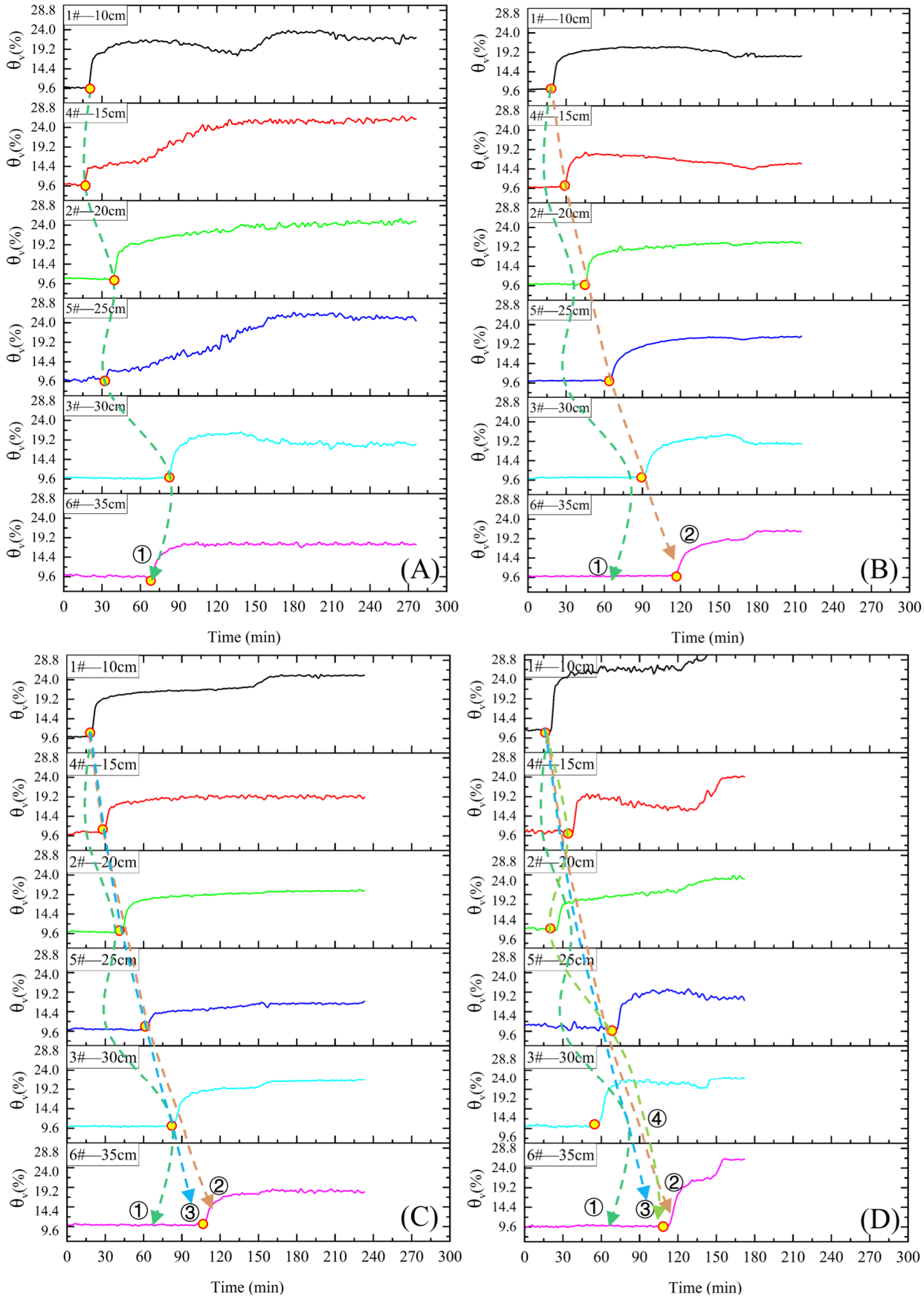


Figure 9. Variation characteristics of volumetric water content in soil with type III root at different times. (Loess with root content of (**A**) 0%, (**B**) 0.23%, (**C**) 1.17% and (**D**) 2.11%).

The volumetric water content of saturated soil under different working conditions will vary with time and depth. In order to explore the effect of root contents and root types on the volumetric water content of saturated soil (i.e., water-holding capacity in soil), we extracted the volume water content of saturated soil under different working conditions, as shown in Figure 10. For loess, the volumetric water content of saturated soil increases first and then decreases with the increase in depth, which may be caused by the upper water supply and the lower water discharge. For the loess with roots, the volumetric water content of saturated soil decreases first and then increases with the increase in depth, which shows that the water-holding capacity of loess with roots is strong.

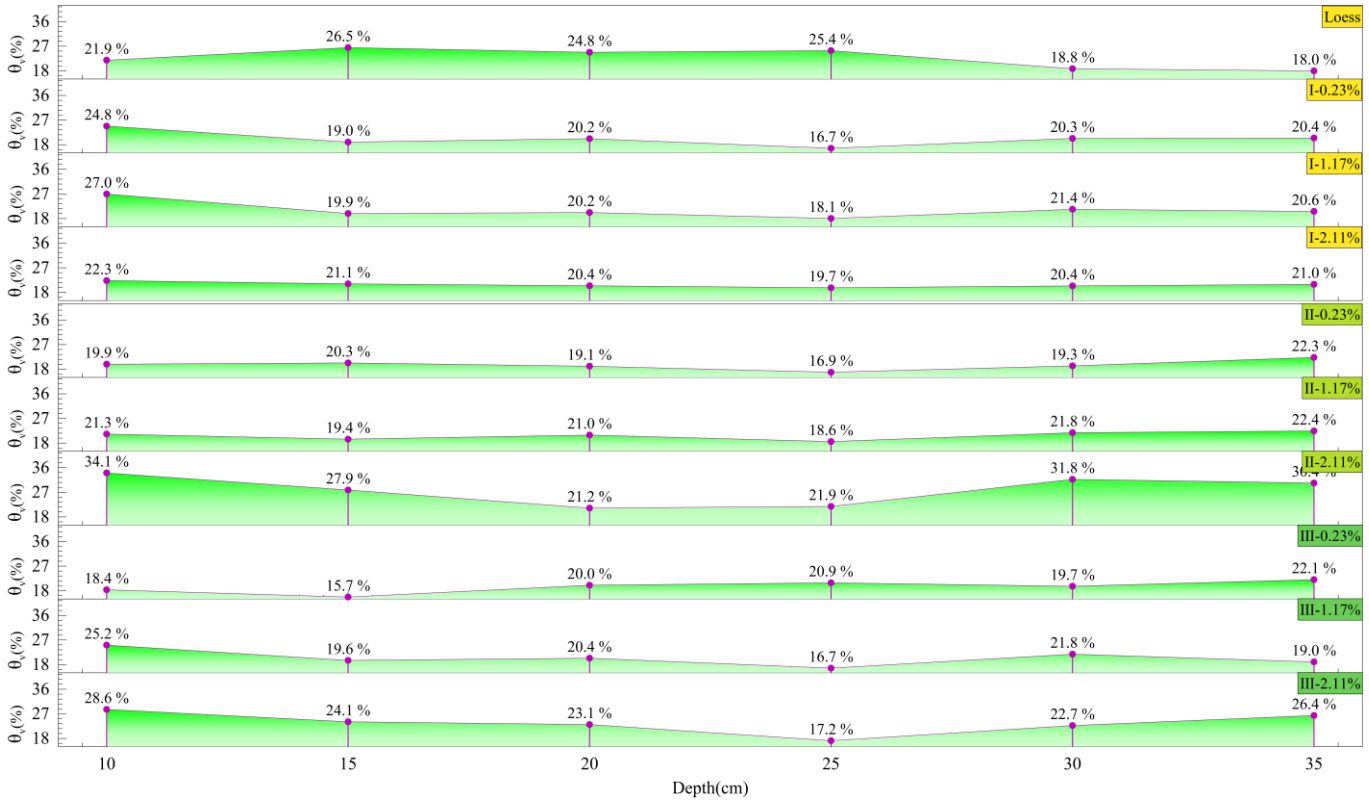


Figure 10. Distribution of water content in saturated loess with different root contents and root types.

In order to investigate the impact of root type and root content on the water-holding capacity of loess with roots, the average values of data from sensors $1^{\#}$–$6^{\#}$ to show the water-holding capacity of this particular type of loess with roots. As depicted in Figure 10, in loess with roots, when the root type remains constant, an increase in root content results in a corresponding augmentation in the average volumetric water content. Consequently, the water-holding capacity of these soils is correspondingly enhanced. Conversely, with a constant root content in loess with roots, in terms of their impact on the average volumetric water content, root types can be ranked in descending order as follows: type II, type III, and type I.

3.3. Effect of Changes in Root Content and Root Type on Saturated Permeability Coefficient

The force on the sensor changes linearly over time after soil is saturated under different working conditions, and the change rate k of force over time can be obtained by using the linear regression method, as shown in Figure 11. According to Equation (6), the variation characteristics of the saturated permeability coefficient K of the soil under different working conditions can be further obtained, as shown in Figure 12.

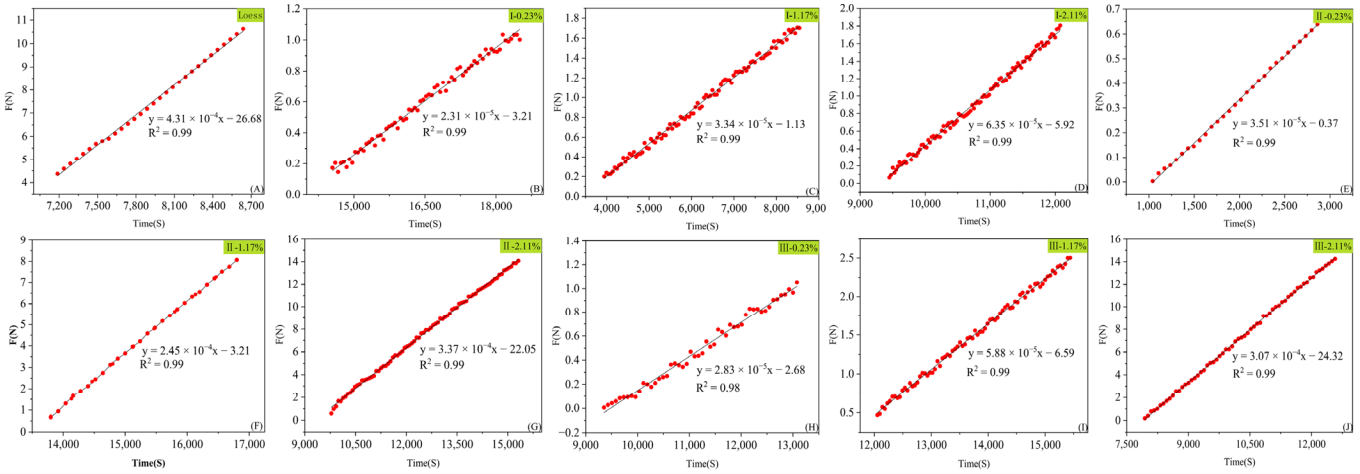


Figure 11. Variation characteristics of force on the sensor over time with different root contents and root types. (**A**) loess; (**B**–**D**) loess containing type I roots with different root contents; (**E**–**G**) loess containing type II roots with different root contents; (**H**–**J**) loess containing type III roots with different root contents.

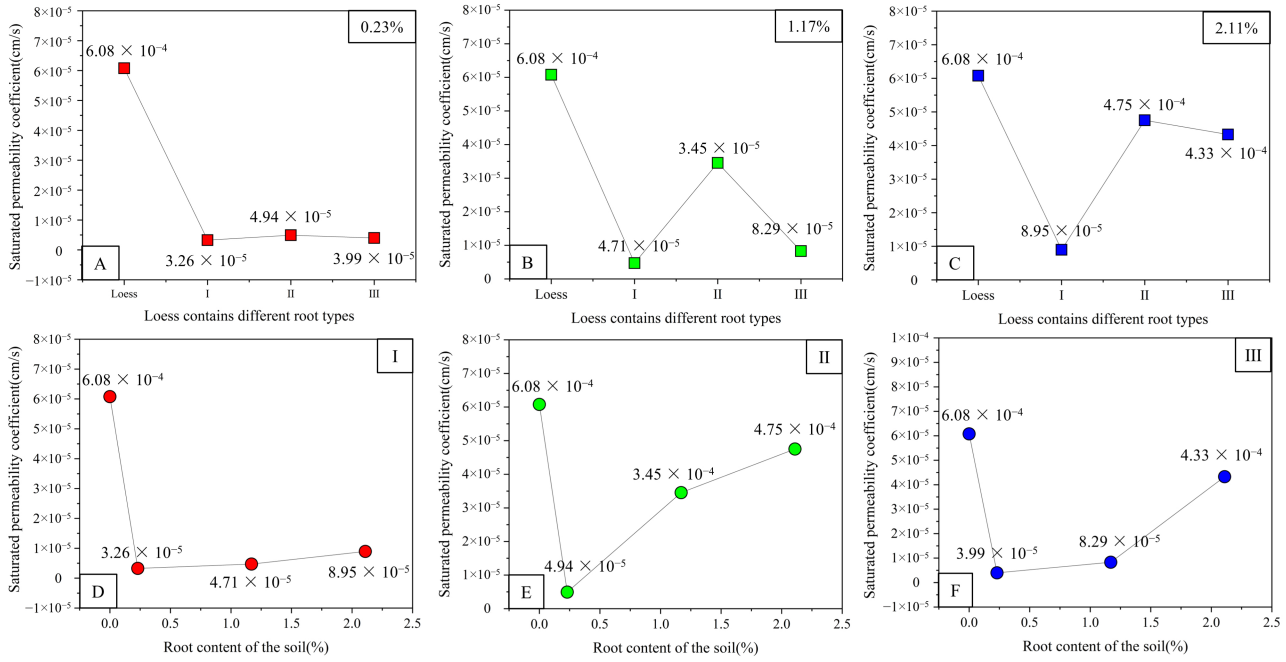


Figure 12. Variation characteristics of the saturated permeability coefficient of soil under different working conditions. The changing characteristics of the migration rate of the wetting front in soil with different root contents (**A**–**C**) and root types (**D**–**F**).

The measured permeability coefficient of loess is 5.95×10^{-4} cm/s, which is consistent with the results obtained by other researchers [38]. This suggests that the modeling device used in this study has sufficient accuracy to meet the test requirements. For loess with roots, an increase in the root content leads to a larger saturated permeability coefficient, while keeping the type of roots constant. Conversely, when the root content is kept constant, loess samples with different root types exhibit the following order of saturated permeability coefficients from largest to smallest: type II, type III, and type I. In loess with roots, when both root content and root type were changed, the soil's saturated permeability coefficient was the largest (4.65×10^{-4} cm/s) with 2.11% root content and type II roots, and the smallest (0.32×10^{-4} cm/s) with 0.23% root content and type I roots.

Table 2 showed the results of calculations with and without considering the effect of "circumferential flow" on the saturated permeability coefficient of the soil. Compared with bare soil, the permeability of loess with roots is lower, which is consistent with the previous results [42]. Notably, method 1 yields a measurement approximately four times higher than method 2.

Table 2. Saturated permeability coefficient of soil, as calculated by different methods.

Soil Type	**Loess with Roots**									**Loess**	**Remarks**
Root Type	**I**			**II**			**III**			**/**	**//**
Root content (%)	0.23	1.17	2.11	0.23	1.17	2.11	0.23	1.17	2.11	/	//
K (10^{-4} cm/s)	0.33	0.47	0.89	0.49	3.45	4.75	0.39	0.83	4.33	6.08	method 1
K' (10^{-4} cm/s)	0.07	0.12	0.23	0.12	0.87	1.25	0.11	0.22	1.19		method 2

Root type II has the greatest effect on the water content and the saturated permeability coefficient of loess with roots when saturated, and we hold that the curvature of roots may be the main reason for such a phenomenon. Therefore, we used a three-dimensional laser scanner (FreeScan UE11) to scan the three-dimensional shape of the root. The scanning process and results are shown in Figure 13A–C. In three-dimensional space, if both ends of the root coincide with the horizontal plane, the length of the root is represented by the length of its central axis L (cm), and the linear length of the root is represented by X (cm), then the formula for calculating the curvature β of the root is expressed in Formula (12). A total of 323 groups of roots were counted this time, and the curvature of different types of roots is shown in Figure 13D. It can be found from the figure that the different types of roots in order of curvature are Type II, Type III and Type I.

$$\beta = \frac{L - X}{L} \tag{12}$$

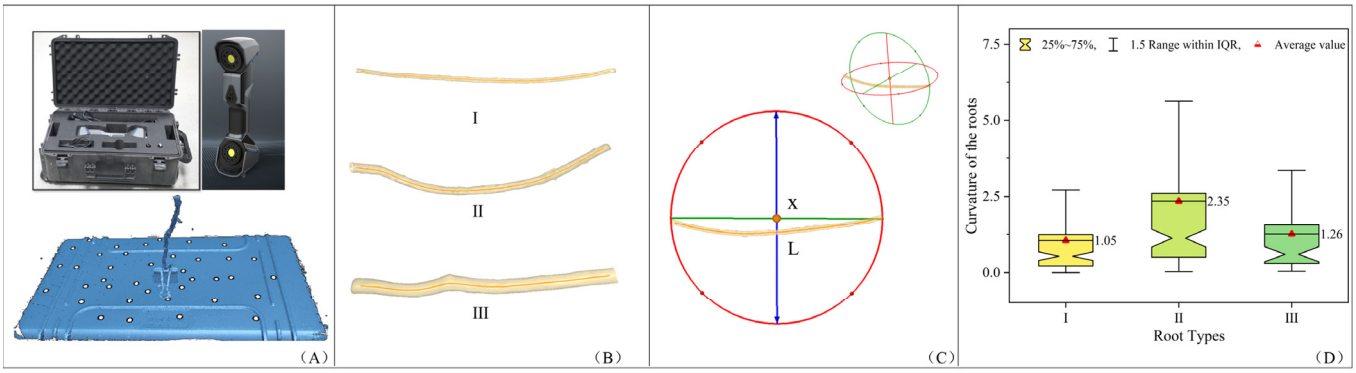


Figure 13. Measurement process in curvature for different types of roots: (**A**) three-dimensional scanning of different types of roots; (**B**) typical three-dimensional shapes of different types of roots; (**C**) calculation of curvature for roots in three-dimensional space; (**D**) statistical results of curvature for different types of roots.

4. Discussion

The study of the morphology and migration law of wetting fronts during water infiltration in loess is vital for predicting the movement of water and solute in soils [43]. In this study, the soil column experiment was performed using a transparent cuboid model device. An interesting finding is that the wetting fronts migrated in a straight line in the cube model box containing loess at constant head height, which is consistent with the results using cylindrical model box under the same conditions [44,45]. This shows that

the shape of the model box had no effect on the migration characteristics of wetting fronts. Nevertheless, the wetting fronts migrated in a semicircular way when water was supplied by the point source method [46,47]. Therefore, the morphology of wetting fronts was mostly affected by the water supply mode.

There is a certain variation law between the saturated permeability coefficient of loess with roots and root type and root content. When the root type is constant and the root content increases, the faster the infiltration rate, the greater the saturated water content (the better the water-holding capacity), and the greater the saturated permeability coefficient; when the root content is constant and the root type changes, the infiltration rate, saturated water content and saturated permeability coefficient of soil are in the following descending order of soils: type II, type III, and type I. The reasons for such changes are as follows: there is no circumferential flow during water infiltration, since there are no roots in the loess. The study results are thus consistent with the previous ones [48,49], as shown in Figure 14A. However, the addition of roots will change the seepage path and the size of cross-section. With the increase in root content, the seepage path remains unchanged, while the cross-section decreases relatively, resulting in a relative increase in the permeability coefficient [50], as shown in Figure 14B–D. When the root content is constant, the change in root type will lead to the changes in both root diameter and number of roots. Therefore, in terms of the number of roots in loess, root types can be ranked in descending order as type I, type II and type III, as shown in Figure 14E–G. According to Equation (11), with the increase in root type, both the cross-section and seepage path at the root will increase, and their relative size leads to a decrease in the saturated permeability coefficient of soils.

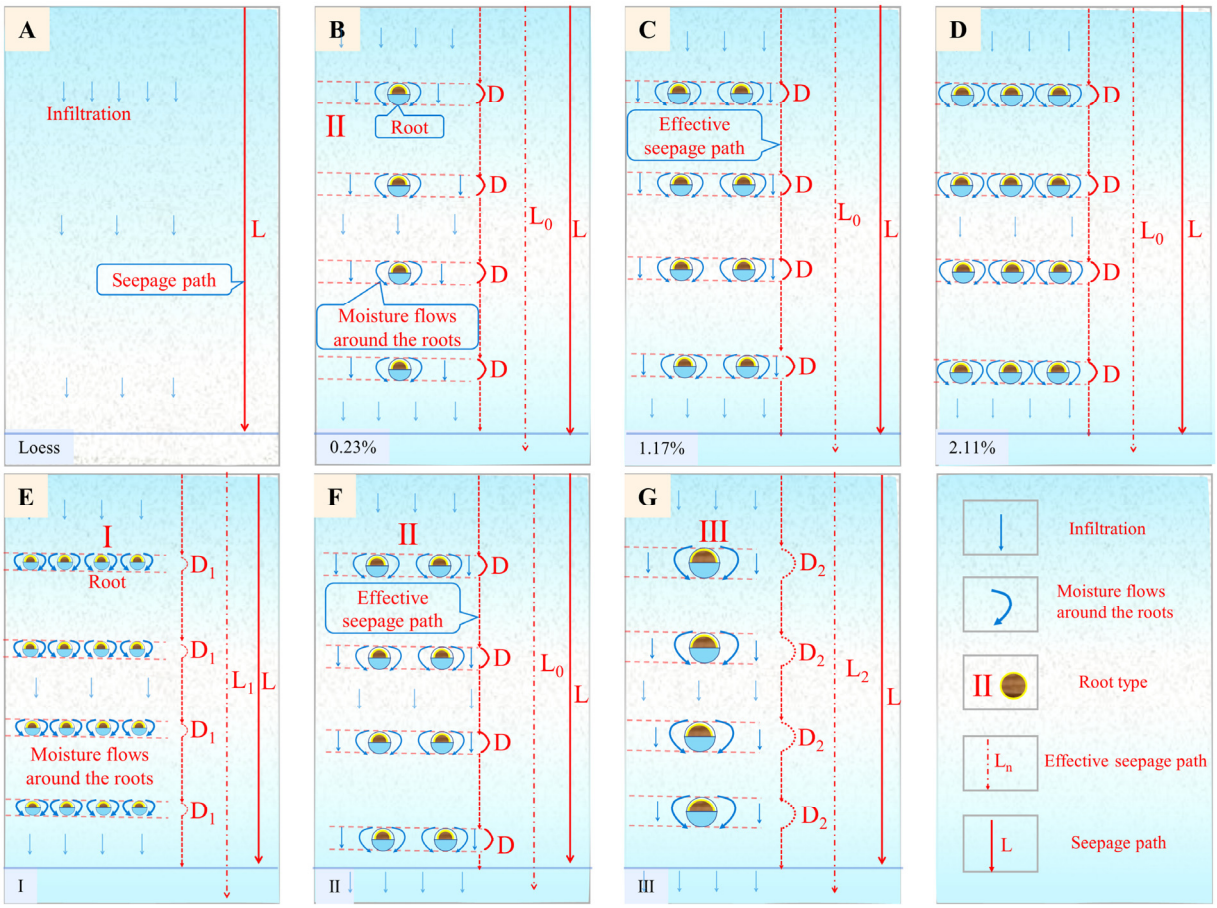


Figure 14. Schematic diagram of water infiltration in loess (**A**); loess with different root contents and the same root type (**B**–**D**); loess with different root types and the same root content (**E**–**G**).

Studies have revealed that with an increase in total porosity, capillary porosity and root mass density, the saturated permeability coefficient of loess increases significantly [51], which is consistent with the results of our study on the effect of root content change on the saturated permeability coefficient. In the field, the permeability coefficient of type I was higher than that of types II and III. This inconsistency with the results of this study is mainly due to changes in the experimental environment [52]. Nonetheless, other studies have shown that both low-density and high-density fine roots (<1 mm) tend to decrease the saturated permeability coefficient, while thick roots (D > 2 mm) tend to increase the saturated permeability coefficient [53]. Meanwhile, changes in soil pores are positively correlated with the infiltration of soil [54]. However, Bodner [55] explored the effect of thick roots and fine roots on the pore size distribution of plants and found that thick roots produced more pores than fine roots. This indirectly proved that thick roots had a greater effect on infiltration than fine roots. This conclusion demonstrates that root types I and III have an impact on the saturated permeability coefficient of soils. However, there is a lack of research on the saturated permeability coefficient of soils with type II roots. Based on the findings of this study, it is believed that the reason for the higher saturated permeability coefficient in soil containing type II roots compared to soil containing type III roots is due to the greater curvature of type II roots. In other words, the equivalent diameter (the diameter formed by the surface layer of the root system at the furthest point from the central axis of the root system) of type II roots is larger than the physical diameter of type III roots.

In this study, the effects of root type and root content on the infiltration characteristics of loess under horizontal distribution were studied quantitatively only by model experiments in the laboratory. Although no systematic studies have been conducted on the roots of other vegetation or their distribution modes, the results of this study can still be used to analyze the effect of the horizontal distribution of roots on water infiltration law and to offer theoretical guidance for water management in agriculture and forestry. In the future, we will consider using a high-density electrical method or thermal imaging method to detect the radius of circumferential flow and further reveal the effect of *Robinia pseudoacacia* species on the law of water infiltration in soil.

5. Conclusions

In this study, a seepage device was used to investigate the water infiltration patterns in loess with roots. The research focused on the impact of changes in root type and root content on water-holding capacity, saturated permeability coefficient, and migration patterns of the wetting front in loess with roots. Furthermore, a three-dimensional laser scanner was used to assess curvature variations among different root types. The main conclusions obtained are as follows:

(1) The morphology of the wetting front during water migration is mainly influenced by the water supply mode; the test device has no impact on the wetting front's morphology.
(2) Root type and content are the primary factors influencing variations in water infiltration rates, soil water-holding capacity, and saturated permeability coefficients in loess with roots.
(3) An increase in root content in loess with the same root type enhances the water infiltration rate, water-holding capacity, and saturated permeability coefficient. When the root content in loess is constant, the impact of root types on the water infiltration rate, water-holding capacity, and saturated permeability coefficient in loess with roots follows a descending order: type II, type III, and type I roots. Root curvature is the primary factor causing these variations.
(4) During water infiltration in loess with roots, there is a phenomenon called "circumferential flow". Changes in root type and root content not only influence variation in the radius of the "circumferential flow" but also contribute to differences in the cross-sectional area and flow paths. Neglecting the "circumferential flow" leads to a larger saturated permeability coefficient for loess with roots.

Author Contributions: Conceptualization, Q.G.; methodology, D.Z. and J.W.; software, T.X. and Q.G.; validation, T.X. and T.G.; formal analysis, D.Z.; investigation, Q.G.; resources, Q.G.; data curation, D.Z.; writing—original draft preparation, Q.G.; writing—review and editing, Q.G. and T.G.; visualization, T.G.; supervision, T.G.; project administration, J.W.; funding acquisition, T.G. All authors have read and agreed to the published version of the manuscript.

Funding: The research presented in this paper was funded by the National Natural Science Foundation of China (42041006 and 42027806).

Data Availability Statement: The data presented in this study are available upon request from the corresponding author.

Conflicts of Interest: The authors declare that they have no conflicts of interest.

References

1. Kroes, J.; van Dam, J.; Supit, I.; de Abelleyra, D.; Verón, S.; de Wit, A.; Boogaard, H.; Angelini, M.; Damiano, F.; Groenendijk, P.; et al. Agrohydrological Analysis of Groundwater Recharge and Land Use Changes in the Pampas of Argentina. *Agric. Water Manag.* **2019**, *213*, 843–857. [CrossRef]
2. Osman, J.R.; Fernandes, G.; DuBow, M.S. Bacterial diversity of the rhizosphere and nearby surface soil of rice (oryza sativa) growing in the camargue (France). *Rhizosphere* **2017**, *3*, 112–122. [CrossRef]
3. Sun, D.; Yang, H.; Guan, D.; Yang, M.; Wu, J.; Yuan, F.; Jin, C.; Wang, A.; Zhang, Y. The Effects of Land Use Change on Soil Infiltration Capacity in China: A Meta-Analysis. *Sci. Total Environ.* **2018**, *626*, 1394–1401. [CrossRef]
4. Yu, X.; Huang, Y.; Li, E.; Li, X.; Guo, W. Effects of Rainfall and Vegetation to Soil Water Input and Output Processes in the Mu Us Sandy Land, Northwest China. *CATENA* **2018**, *161*, 96–103. [CrossRef]
5. Asseng, S.; Ritchie, J.T.; Smucker, A.J.M.; Robertson, M.J. Root Growth and Water Uptake during Water Deficit and Recovering in Wheat. *Plant Soil* **1998**, *201*, 265–273. [CrossRef]
6. Bordoni, M.; Meisina, C.; Valentino, R.; Lu, N.; Bittelli, M.; Chersich, S. Hydrological Factors Affecting Rainfall-Induced Shallow Landslides: From the Field Monitoring to a Simplified Slope Stability Analysis. *Eng. Geol.* **2015**, *193*, 19–37. [CrossRef]
7. Pandey, P.K.; Pandey, V. Estimation of Infiltration Rate from Readily Available Soil Properties (RASPs) in Fallow Cultivated Land. *Sustain. Water Resour. Manag.* **2019**, *5*, 921–934. [CrossRef]
8. Wang, Y.; Hu, W.; Zhu, Y.; Shao, M.; Xiao, S.; Zhang, C. Vertical Distribution and Temporal Stability of Soil Water in 21-m Profiles under Different Land Uses on the Loess Plateau in China. *J. Hydrol.* **2015**, *527*, 543–554. [CrossRef]
9. Cosgrove, W.J.; Loucks, D.P. Water Management: Current and Future Challenges and Research Directions. *Water Resour. Res.* **2015**, *51*, 4823–4839. [CrossRef]
10. Bens, O.; Wahl, N.A.; Fischer, H.; Hüttl, R.F. Water Infiltration and Hydraulic Conductivity in Sandy Cambisols: Impacts of Forest Transformation on Soil Hydrological Properties. *Eur. J. Forest Res.* **2007**, *126*, 101–109. [CrossRef]
11. Gu, C.; Mu, X.; Gao, P.; Zhao, G.; Sun, W.; Tatarko, J.; Tan, X. Influence of Vegetation Restoration on Soil Physical Properties in the Loess Plateau, China. *J. Soils Sediments* **2019**, *19*, 716–728. [CrossRef]
12. Zaheer, M.; Wen, Z.; Zhan, H.; Chen, X.; Jin, M. An Experimental Study on Solute Transport in One-Dimensional Clay Soil Columns. *Geofluids* **2017**, *2017*, e6390607. [CrossRef]
13. Zhai, Y.; Kurexi, W.; Wang, C.; Zhu, C.; Zhang, Z.; Li, Y. Modelling Soil Water Infiltration and Wetting Patterns in Variable Working-Head Moistube Irrigation. *Agronomy* **2023**, *13*, 2987. [CrossRef]
14. Fatehnia, M.; Tawfiq, K.; Ye, M. Estimation of Saturated Hydraulic Conductivity from Double-Ring Infiltrometer Measurements. *Eur. J. Soil Sci.* **2016**, *67*, 135–147. [CrossRef]
15. Gill, M.A. Analysis of Permeameter Data to Obtain Parameters of Non-Darcy Flow. *J. Hydrol.* **1977**, *32*, 165–173. [CrossRef]
16. Joel, A.; Messing, I. Infiltration Rate and Hydraulic Conductivity Measured with Rain Simulator and Disc Permeameter on Sloping Arid Land. *Arid. Land Res. Manag.* **2001**, *15*, 371–384. [CrossRef]
17. Schiettecatte, W.; Jin, K.; Yao, Y.; Cornelis, W.M.; Lu, J.; Wu, H.; Verbist, K.; Cai, D.; Gabriels, D.; Hartmann, R. Influence of Simulated Rainfall on Physical Properties of a Conventionally Tilled Loess Soil. *CATENA* **2005**, *64*, 209–221. [CrossRef]
18. Peng, Y.; Fei, L.; Jie, F.; Hao, K.; Liu, L.; Shen, F.; Fan, Q. Effects of Bio-Organic Fertilizer on Soil Infiltration, Water Distribution, and Leaching Loss under Muddy Water Irrigation Conditions. *Agronomy* **2023**, *13*, 2014. [CrossRef]
19. Ruggenthaler, R.; Meißl, G.; Geitner, C.; Leitinger, G.; Endstrasser, N.; Schöberl, F. Investigating the Impact of Initial Soil Moisture Conditions on Total Infiltration by Using an Adapted Double-Ring Infiltrometer. *Hydrol. Sci. J.* **2016**, *61*, 1263–1279. [CrossRef]
20. Fu, Q.; Hou, R.; Li, T.; Li, Y.; Liu, D.; Li, M. A New Infiltration Model for Simulating Soil Water Movement in Canal Irrigation under Laboratory Conditions. *Agric. Water Manag.* **2019**, *213*, 433–444. [CrossRef]
21. Huang, J.; Wu, P.; Zhao, X. Effects of Rainfall Intensity, Underlying Surface and Slope Gradient on Soil Infiltration under Simulated Rainfall Experiments. *CATENA* **2013**, *104*, 93–102. [CrossRef]
22. Minasny, B.; McBratney, A.B. Estimation of Sorptivity from Disc-Permeameter Measurements. *Geoderma* **2000**, *95*, 305–324. [CrossRef]

23. Barry, D.A. Effect of Nonuniform Boundary Conditions on Steady Flow in Saturated Homogeneous Cylindrical Soil Columns. *Adv. Water Resour.* **2009**, *32*, 522–531. [CrossRef]
24. Kalbe, U.; Bandow, N.; Bredow, A.; Mathies, H.; Piechotta, C. Column Leaching Tests on Soils Containing Less Investigated Organic Pollutants. *J. Geochem. Explor.* **2014**, *147*, 291–297. [CrossRef]
25. Naka, A.; Yasutaka, T.; Sakanakura, H.; Kalbe, U.; Watanabe, Y.; Inoba, S.; Takeo, M.; Inui, T.; Katsumi, T.; Fujikawa, T.; et al. Column Percolation Test for Contaminated Soils: Key Factors for Standardization. *J. Hazard. Mater.* **2016**, *320*, 326–340. [CrossRef] [PubMed]
26. Mao, L.L.; Lei, T.W.; Bralts, V.F. An Analytical Approximation Method for the Linear Source Soil Infiltrability Measurement and Its Application. *J. Hydrol.* **2011**, *411*, 169–177. [CrossRef]
27. Su, N. Radial Water Infiltration–Advance–Evaporation Processes during Irrigation Using Point Source Emitters in Rigid and Swelling Soils. *J. Hydrol.* **2007**, *344*, 190–197. [CrossRef]
28. Wang, X.; Geng, L.; Zhou, H.; Huang, Y.; Ji, J. Effects of Subsoiling with Different Wing Mounting Heights on Soil Water Infiltration Using HYDRUS-2D Simulations. *Agronomy* **2023**, *13*, 2742. [CrossRef]
29. Morillon, R.; Lassalles, J.-P. Water Deficit during Root Development: Effects on the Growth of Roots and Osmotic Water Permeability of Isolated Root Protoplasts. *Planta* **2002**, *214*, 392–399. [CrossRef]
30. Archer, N.A.L.; Otten, W.; Schmidt, S.; Bengough, A.G.; Shah, N.; Bonell, M. Rainfall Infiltration and Soil Hydrological Characteristics below Ancient Forest, Planted Forest and Grassland in a Temperate Northern Climate. *Ecohydrology* **2016**, *9*, 585–600. [CrossRef]
31. Fischer, C.; Tischer, J.; Roscher, C.; Eisenhauer, N.; Ravenek, J.; Gleixner, G.; Attinger, S.; Jensen, B.; de Kroon, H.; Mommer, L.; et al. Plant Species Diversity Affects Infiltration Capacity in an Experimental Grassland through Changes in Soil Properties. *Plant Soil* **2015**, *397*, 1–16. [CrossRef]
32. Cui, Z.; Wu, G.-L.; Huang, Z.; Liu, Y. Fine Roots Determine Soil Infiltration Potential than Soil Water Content in Semi-Arid Grassland Soils. *J. Hydrol.* **2019**, *578*, 124023. [CrossRef]
33. Liu, Y.; Cui, Z.; Huang, Z.; López-Vicente, M.; Wu, G.-L. Influence of Soil Moisture and Plant Roots on the Soil Infiltration Capacity at Different Stages in Arid Grasslands of China. *CATENA* **2019**, *182*, 104147. [CrossRef]
34. Yang, H.; Gao, J.; Pan, C.; Qing, S.; Wu, Y.; Jiang, L.; Wang, Z.; Wang, D. Species Composition and Influencing Factors of Understory Woody Species in *Robinia pseudoacacia* Plantations on the Loess Plateau. *J. For. Res.* **2023**, *34*, 1693–1706. [CrossRef]
35. Wang, B.; Liu, G.; Xue, S. Effect of Black Locust (*Robinia pseudoacacia*) on Soil Chemical and Microbiological Properties in the Eroded Hilly Area of China's Loess Plateau. *Environ. Earth Sci.* **2012**, *65*, 597–607. [CrossRef]
36. Benesperi, R.; Giuliani, C.; Zanetti, S.; Gennai, M.; Mariotti Lippi, M.; Guidi, T.; Nascimbene, J.; Foggi, B. Forest Plant Diversity Is Threatened by *Robinia pseudoacacia* (Black-Locust) Invasion. *Biodivers. Conserv.* **2012**, *21*, 3555–3568. [CrossRef]
37. Vítková, M.; Sádlo, J.; Roleček, J.; Petřík, P.; Sitzia, T.; Müllerová, J.; Pyšek, P. *Robinia pseudoacacia*-Dominated Vegetation Types of Southern Europe: Species Composition, History, Distribution and Management. *Sci. Total Environ.* **2020**, *707*, 134857. [CrossRef] [PubMed]
38. Liang, H.; Xue, Y.; Li, Z.; Wang, S.; Wu, X.; Gao, G.; Liu, G.; Fu, B. Soil Moisture Decline Following the Plantation of *Robinia pseudoacacia* Forests: Evidence from the Loess Plateau. *Forest Ecol. Manag.* **2018**, *412*, 62–69. [CrossRef]
39. Kou, M.; Garcia-Fayos, P.; Hu, S.; Jiao, J. The Effect of *Robinia pseudoacacia* Afforestation on Soil and Vegetation Properties in the Loess Plateau (China): A Chronosequence Approach. *Forest Ecol. Manag.* **2016**, *375*, 146–158. [CrossRef]
40. Gambill, D.R.; Wall, W.A.; Fulton, A.J.; Howard, H.R. Predicting USCS Soil Classification from Soil Property Variables Using Random Forest. *J. Terramechanics* **2016**, *65*, 85–92. [CrossRef]
41. Liu, Y.; Wang, G.; Yu, K.; Li, P.; Xiao, L.; Liu, G. A New Method to Optimize Root Order Classification Based on the Diameter Interval of Fine Root. *Sci. Rep.* **2018**, *8*, 2960. [CrossRef] [PubMed]
42. Leung, A.K.; Garg, A.; Coo, J.L.; Ng, C.W.W.; Hau, B.C.H. Effects of the Roots of Cynodon Dactylon and Schefflera Heptaphylla on Water Infiltration Rate and Soil Hydraulic Conductivity. *Hydrol. Process.* **2015**, *29*, 3342–3354. [CrossRef]
43. de Rooij, G.H. Modeling Fingered Flow of Water in Soils Owing to Wetting Front Instability: A Review. *J. Hydrol.* **2000**, *231–232*, 277–294. [CrossRef]
44. Dong, X.; Liu, X.; Woo, H.; Park, J. A Developed Soil Column Test Device for Measuring the Electrical Conductivity Breakthrough Curves. *Environ. Earth Sci.* **2014**, *72*, 3715–3722. [CrossRef]
45. Montoya-Dominguez, J.D.; García-Aristizábal, E.F.; Vega-Posada, C.A. One-Dimensional Experimental Study of Rainfall Infiltration into Unsaturated Soil. *Rev. Fac. Ing. Univ. Antioquia* **2017**, *82*, 74–81. [CrossRef]
46. Revol, P.; Clothier, B.E.; Mailhol, J.-C.; Vachaud, G.; Vauclin, M. Infiltration from a Surface Point Source and Drip Irrigation: 2. An Approximate Time-Dependent Solution for Wet-Front Position. *Water Resour. Res.* **1997**, *33*, 1869–1874. [CrossRef]
47. Zhang, R.; Cheng, Z.; Zhang, J.; Ji, X. Sandy Loam Soil Wetting Patterns of Drip Irrigation: A Comparison of Point and Line Sources. *Procedia Eng.* **2012**, *28*, 506–511. [CrossRef]
48. van Schaik, N.L.M.B. Spatial Variability of Infiltration Patterns Related to Site Characteristics in a Semi-Arid Watershed. *CATENA* **2009**, *78*, 36–47. [CrossRef]
49. Zhang, W.; Ahanbieke, P.; Wang, B.J.; Xu, W.L.; Li, L.H.; Christie, P.; Li, L. Root Distribution and Interactions in Jujube Tree/Wheat Agroforestry System. *Agroforest. Syst.* **2013**, *87*, 929–939. [CrossRef]

50. Wang, L.; Zhong, C.; Gao, P.; Xi, W.; Zhang, S. Soil Infiltration Characteristics in Agroforestry Systems and Their Relationships with the Temporal Distribution of Rainfall on the Loess Plateau in China. *PLoS ONE* **2015**, *10*, e0124767. [CrossRef]
51. Zhu, P.; Zhang, G.; Zhang, B. Soil Saturated Hydraulic Conductivity of Typical Revegetated Plants on Steep Gully Slopes of Chinese Loess Plateau. *Geoderma* **2022**, *412*, 115717. [CrossRef]
52. Webb, B.; Robinson, D.A.; Marshall, M.R.; Ford, H.; Pagella, T.; Healey, J.R.; Smith, A.R. Variation in Root Morphology amongst Tree Species Influences Soil Hydraulic Conductivity and Macroporosity. *Geoderma* **2022**, *425*, 116057. [CrossRef]
53. Lu, J.; Zhang, Q.; Werner, A.D.; Li, Y.; Jiang, S.; Tan, Z. Root-Induced Changes of Soil Hydraulic Properties—A Review. *J. Hydrol.* **2020**, *589*, 125203. [CrossRef]
54. Ma, J.; Zeng, R.; Yao, Y.; Meng, X.; Meng, X.; Zhang, Z.; Wang, H.; Zhao, S. Characterization and Quantitative Evaluation of Preferential Infiltration in Loess, Based on a Soil Column Field Test. *CATENA* **2022**, *213*, 106164. [CrossRef]
55. Bodner, G.; Leitner, D.; Kaul, H.-P. Coarse and Fine Root Plants Affect Pore Size Distributions Differently. *Plant Soil* **2014**, *380*, 133–151. [CrossRef] [PubMed]

Disclaimer/Publisher's Note: The statements, opinions and data contained in all publications are solely those of the individual author(s) and contributor(s) and not of MDPI and/or the editor(s). MDPI and/or the editor(s) disclaim responsibility for any injury to people or property resulting from any ideas, methods, instructions or products referred to in the content.